

INFLUENCE OF STRESS CORROSION CRACK MORPHOLOGY ON ULTRASONIC EXAMINATION PERFORMANCES

Authors : Olivier Dupond¹, Thierry Fouquet², Jorge Tirira³,

¹ EDF R&D/Material and Mechanic of Components Department, 77818 Moret-sur-Loing, France

² EDF R&D/SINETICS Department, 92141 Clamart, France

³ CEA/LIST, 91191 Saclay, France

ABSTRACT

Stress Corrosion Cracking represents a potential damage for several components in PWR. For this reason, NDE of stress corrosion cracks corresponds to an important stake for Electricité de France (EDF) both for the availability and for the safety of plants.

SCC crack encountered for Ni-based components in primary coolant medium usually presents an intergranular propagation. The degradation mechanism then induces morphological specificities of the defect, such as rugosity or branched characteristics. Compared with fatigue cracks, SCC morphology may then have an effect on NDE performances, both in terms of detection and characterisation of the defect.

The goal of this paper is to evaluate the influence of the stress corrosion crack morphology on the ultrasonic inspection. The study mixes an experimental approach conducted on artificial flaws - supposed to represent the morphologic features of SCC cracks - and a modelling approach with the 2D finite elements code ATHENA 2D developed by EDF, the semi-analytical code CIVA developed by CEA/LIST and an hybrid code coupling semi-analytical and finite elements code, developed by EDF and CEA. By comparison of experimental and modelling results, the beam-defect interaction in models is validated for complex 2D defects. The interest of modelling is then illustrated with the analysis of specific ultrasonic response observed experimentally for different defects and reproduced with modelling.

1. INTRODUCTION

Ultrasonic simulation tools aim at conceiving or at optimizing inspection characteristics as well as at qualifying inspection procedures or at allowing interpretations of results. UT simulation tools include beam propagation and flaw scattering for various probes (contact or immersion), flaws and materials (homogeneous or heterogeneous structures made of isotropic or anisotropic media). Thanks to the constant developments of the modelling, the studied configurations are more and more complex. This paper is dedicated to the modelling of complex flaw scattering.

EDF (Electricité de France) has experienced primary water stress corrosion cracking (PWSCC) on various number of components of Pressurized Water Reactors (PWR) : for examples CRDMs [1] or Steam Generator Divider Plate [2]. Due to the inter-granular crack propagation mechanism, the defect presents a specific morphology which can be described as multifaceted and branched. As a consequence, this defect morphology may have an effect on the performances of ultrasonic inspection. A previous paper was dedicated to the comparison of experiences and ATHENA finite elements code [3]. The goal of the present paper is to compare different codes and their ability to simulate the complex flaw scattering. Three codes are evaluated : CIVA UT simulation semi-analytical code, ATHENA finite element code and a recent hybrid code coupling semi-analytical and finite element codes [4]. This study is limited to isotropic and homogeneous structure, and to compression waves.

2. BASIC PRINCIPLES OF MODELLING CODES

This part of the document presents briefly the different approaches of the three codes evaluated in the study.

2.1. CIVA UT simulation approach

The ultrasonic modelling tools in CIVA rely on semi-analytical solutions to compute the ultrasonic beam inside the component and its interaction with flaws. For beam propagation simulation, a so-called ‘pencil method’ [5] is used, which consists of meshing the probe as a set of individual source points which radiate spherical longitudinal waves in the coupling or solid wedge and integrating those elementary contributions. Flaw response is computed using different modelling approaches depending upon the technique (TOFD or pulse-echo mode) and upon the flaw (void or inclusion). Indeed, different echo formations are involved : specular (or nearly specular) reflection, edges diffraction, partial transmission or reflection (on solid inclusion in host medium). According to those different interactions, dedicated approaches are used : Kirchhoff approximation for direct or corner echo in nearly specular modes [6], GTD (Geometrical Theory of Diffraction) for edges diffraction echoes, and Born (modified) for solid inclusion response simulation. Finally, the Auld’s reciprocity theorem is used to predict the echo at reception.

2.2. ATHENA finite element model characteristics

ATHENA 2D is a finite elements code for elastodynamics developed by EDF (Electricité de France) Research and Development in collaboration with INRIA [7]. The model uses a regular mesh for the component. Contact and immersed transducers are implemented. Calculations can be performed for all type of structures, especially anisotropic and heterogeneous structures [8] and take into account wave attenuation due to grain scattering [9]. The beam propagation and beam to defect interactions are calculated with all conversion modes. Furthermore, defects are represented with the fictitious domain method which gives the opportunity to separate the defect and the component meshes. Recent developments have been performed to implement branched and multifaceted defects.

2.3. Hybrid method coupling semi-analytical and finite-element codes

In addition to existing models, a hybrid method based on the coupling of semi-analytical beam computation technique and the FEM ATHENA used for exact flaw scattering calculation and should be soon added in a new version of CIVA. The interest of such an approach is to join the advantages of each model : fast 3D beam propagation calculation of the semi-analytical code and exact flaw scattering calculation for the FEM code.

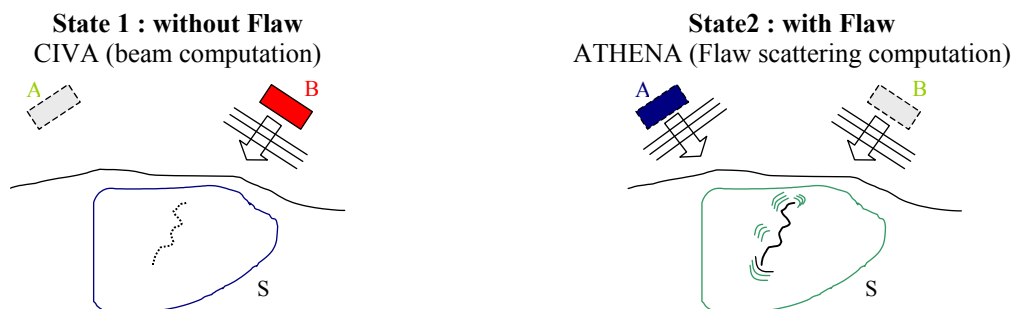


Figure 1 : Schematic illustration of the Auld’s reciprocity principle applied to the hybrid code.

This hybrid simulation tool is already available for 2D applications, while its extension to 3D is under progress [10]. The coupling method is based on the Auld's reciprocity principle [11], assuming two different states illustrated on Figure 1 : in state 1, one probe is acting as a transmitter, and the second one as a receiver, and no flaw is present, while in state 2, a flaw is present, and the operating modes of the probe are reversed. The Auld's reciprocity derived to its transient form [4] allows to calculate the received signal $s(t)$:

$$s(t) = \frac{1}{4P} \iint_s [(h v_i^{(1)} * \sigma_{ij}^{(2)})(t) - (v_i^{(2)} * h \sigma_{ij}^{(1)})(t)] h_j dS \quad (1)$$

where $h v_i^{(1)}$ and $h \sigma_{ij}^{(1)}$ denote respectively the impulse responses for velocity and stresses, calculated by the beam computation in CIVA, whereas $h v_i^{(2)}$ and $\sigma_{ij}^{(2)}$ denote the velocity and stresses as computed by the FEM code in presence of the flaw and P is the normalisation power factor.

3. MOCK-UPS AND DEFECTS DESCRIPTION

The goal of this study is firstly to evaluate experimentally the influence of morphological characteristics of defects on the UT performances and secondly to have experimental results for comparison with modelling results. So the study is performed on machined and calibrated defects.

Figures 2 and 3 present the mock-ups used in the study. Seven defects are electro-eroded in two flat mock-ups. The base material is a forged austenitic stainless steel, type AISI 316L. The thickness of the mock-ups is equal to 38 mm. Each defect is 0.35 mm wide. Defect A is the reference defect consisting of a straight notch. Defects B, C and D are composed of a number of facets respectively equal to 5, 10 and 20. In each case, the facets have a tilted angle of $\pm 14^\circ$ compared to the vertical. The last three defects, E, F and G, are branched. Defects E and F have a Y shape. The intersection point is respectively located at 8 and 5 mm from the inner surface. The angle between the upper branches is equal to 90° . Finally, defect G is composed of a primary notch of 10 mm height and a secondary branch tilted with an angle of 45° , intercepting the primary branch at 5 mm from the inner surface. The tip of the secondary branch is located at 7 mm from the inner surface.

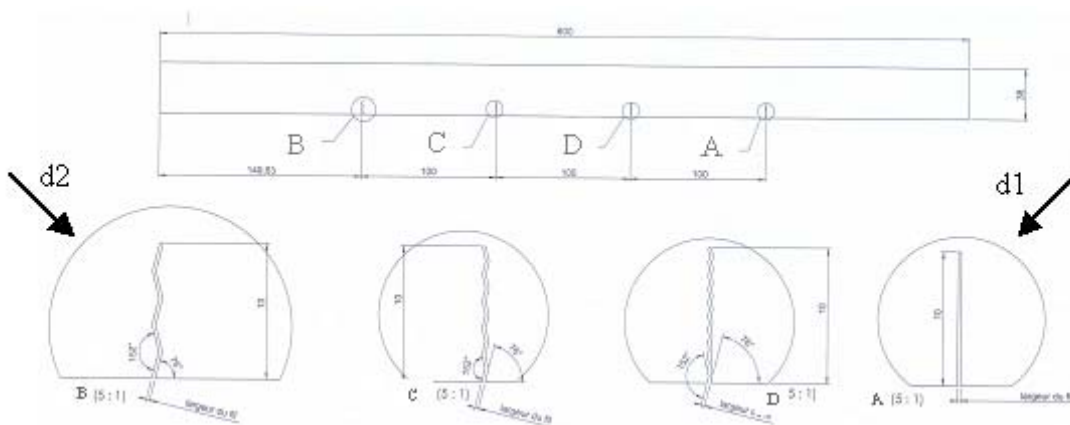


Figure 2 : Mock-up n°1 with machined notches: reference notch and multi faceted notches and inspection direction (d1 and d2).

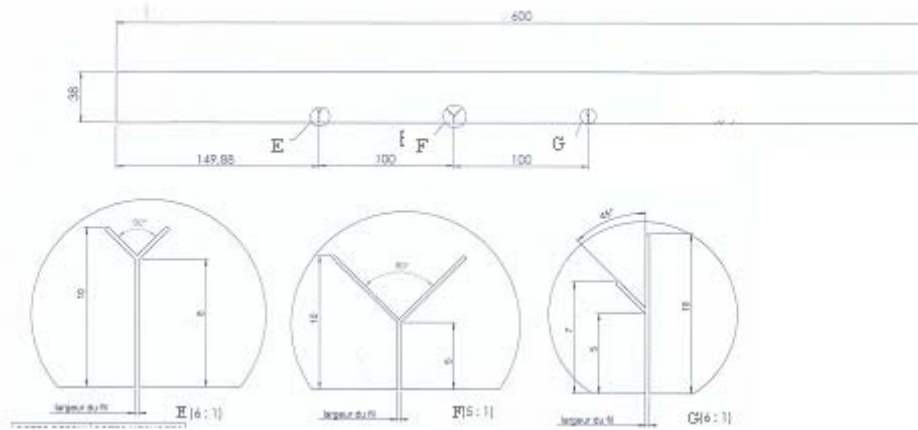


Figure 3 : Mock-up n°2 with branched notches.

4. MODELLING OF COMPLEX FLAW SCATTERING CONFIGURATIONS

4.1. Modelling of corner echo detection for multi faceted defects

Firstly, the multi faceted defects are analysed. Figure 4 presents experimental B-scan images for a 45° compression waves (CW) planar contact transducer with a frequency equal to 2.25 MHz. For each defect, the amplitude of the corner echo is reported in Tables I and II respectively for 45° and 60° refracted angle. The reference defect is a side-drilled hole of 1.5 mm diameter located at 40 mm depth. Whenever multi faceted defects are inspected, experiments have demonstrated a significant variation of the amplitude of the corner echo and the presence of intermediate echoes between the corner echo and the tip diffraction echoes, depending on the number of facets [3].

In the following approach, as all defects are machined all along the width of the mock-ups, 2D versions of ATHENA and of the hybrid code can be used to simulate these specific configurations of inspection. Simulation of the interaction between incident wave and flaw is performed in 3D with CIVA software, and 2D with ATHENA FEM code and the hybrid method.

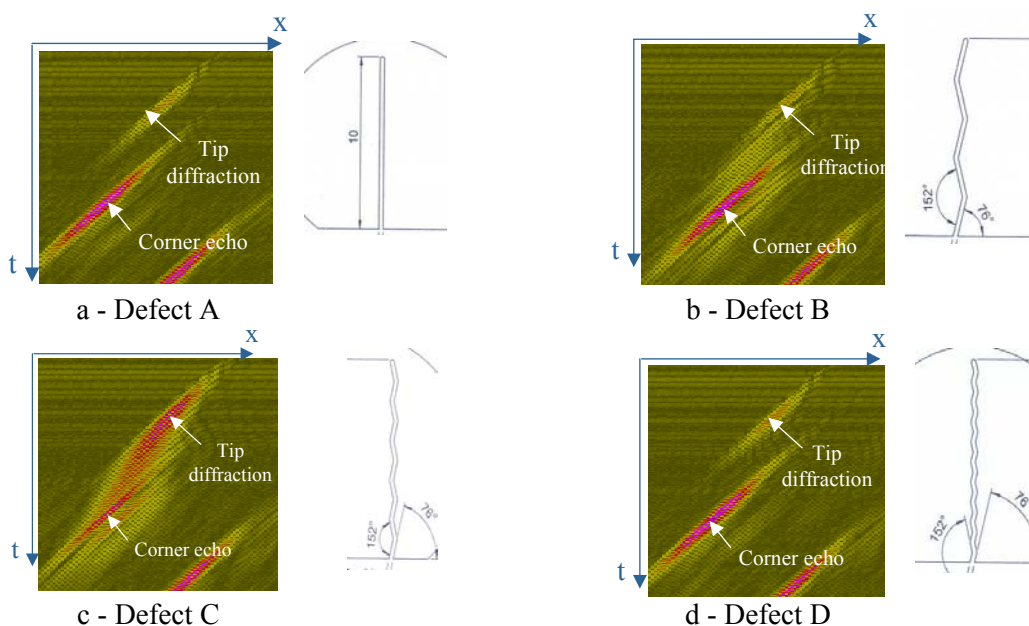


Figure 4 : Experimental B-scan image for 45° CW contact transducer.

Table I : Estimated amplitude of the corner echo (dB) for CW45°.

Defect	Direction of inspection d1				Direction of inspection d2			
	Experiment	CIVA	ATHENA	Hybrid	Experiment	CIVA	ATHENA	Hybrid
	A (dB)	A (dB)	A (dB)	A (dB)	A (dB)	A (dB)	A (dB)	A (dB)
A	3.0	4.5	2.5	4.0	4.0	4.5	2.5	4.0
B	4.0	5.0	4.0	5.0	4.5	4.5	4.5	4.5
C	1.0	0.5	1.5	1.0	6.5	8.0	5.5	7.5
D	4.0	5.5	3.0	4.5	3.0	5.0	2.5	3.5

Table II : Estimated amplitude of the corner echo (dB) for CW 60°.

Defect	Direction of inspection d1				Direction of inspection d2			
	Experiment	CIVA	ATHENA	Hybrid	Experiment	CIVA	ATHENA	Hybrid
	A (dB)	A (dB)	A (dB)	A (dB)	A (dB)	A (dB)	A (dB)	A (dB)
A	4.5	5.5	3.5	5.5	5.0	5.5	3.5	5.5
B	4.0	5.5	4.0	6.0	7.0	6.5	6.0	7.0
C	5.5	3.0	3.5	4.5	5.5	8.5	5.5	8.0
D	4.5	6.0	3.5	5.5	4.0	5.0	3.5	4.5

The Figure 5 presents B scan images for compression waves refracted at 45° for defects C and D. This figure illustrates the influence of the number of facets on the number of echoes. A good qualitative agreement between modelling and experiment is observed.

Quantitatively, for the CW 45° configuration, the variation of the amplitude of the corner is correctly reproduced with each modelling code. In particular, for defect C, the dependence of the amplitude with the direction of control is predicted.

In the case of CW 60°, experimental results show sensitivity to the direction of inspection for the defect B, which is better reproduced with ATHENA. Besides, all simulations give a difference between d1 and d2 for the defect C, not observed experimentally.

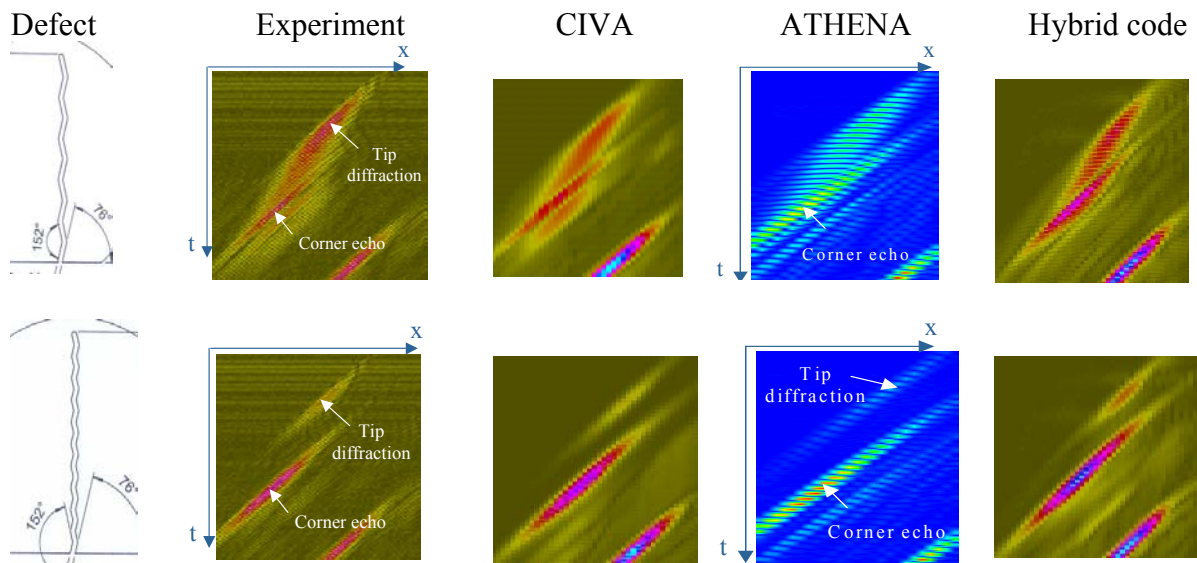


Figure 5 : Comparison of experimental and modelling B-scan images for 45° CW contact transducer (defect C and D).

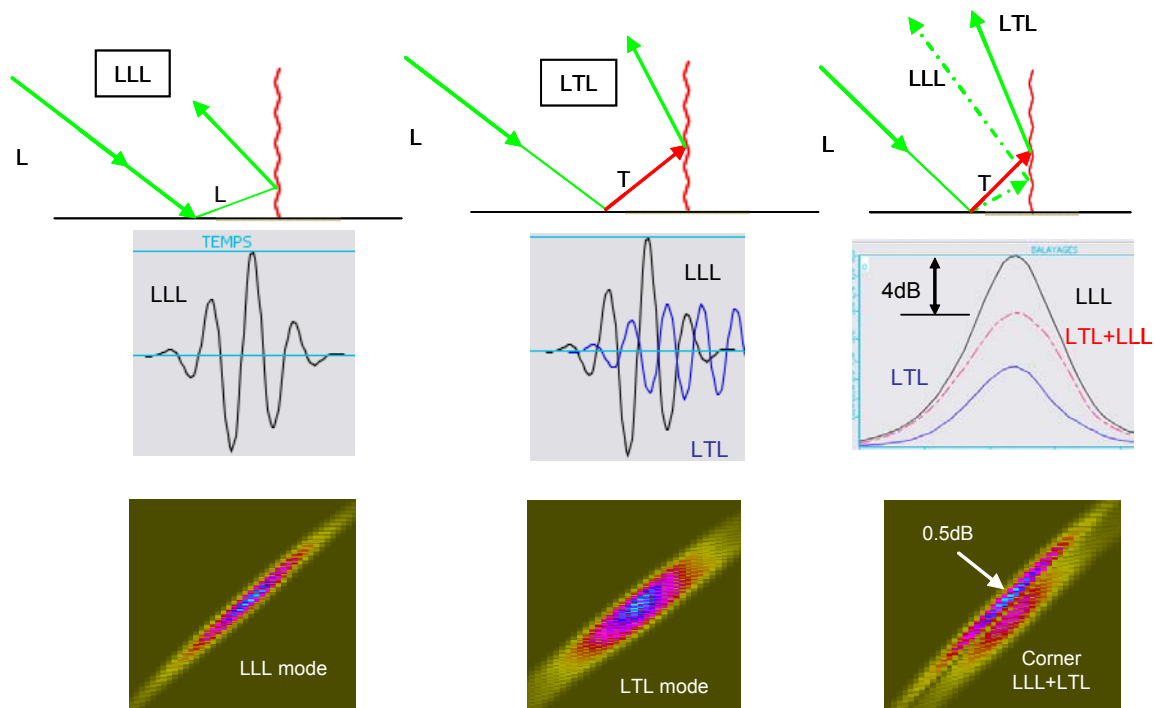


Figure 6 : Mode decomposition with CIVA software for defect C in direction d1.

The origin of the vanishing of the intermediate echoes for the defect D was explained in a previous paper [3] thanks to the visualization of snapshots for different time of flight in ATHENA code. Presently, the decrease of the amplitude of the corner echo on the defect C with CW 45° in direction d1 is explained by a mode decomposition with CIVA software. Results are presented on Figure 6. It suggests that a destructive combination of LLL and LTL modes induces the decrease of the amplitude of the corner echo.

4.2. Modelling the inspection of branched defects

In this part, performances of the codes for modelling the interaction with the branch defects are evaluated.

The Figure 7 presents B-scan images for CW 45° inspection of defects E, F and G. By comparison with experiments, the interaction with the defect is qualitatively correctly reproduced with codes : presence of a tip diffraction on the left branch, identification of a specular echo on the right one, an echo due to multiple reflections between the two branches for the defect G and an additional echo in the vicinity of the corner echo resulting from an interaction of the beam with the left branch.

Amplitudes of all echoes, except the echo after skip, are reported in table III.

For branched defects, as far as the corner echo is concerned, the amplitude is correctly reproduced with all codes except for the defect F which presents with ATHENA an underestimation of 5 dB compared with the experimental result. Actually, a specific analysis has been undergone for this configuration. The origin of this difference is attributed to the small differences that can exist in the description of the transducer in the model, for example the beam opening (11.2 mm instead of 9.6 mm). For this specific configuration, it induces a significant difference on the amplitude of the corner echo. To confirm this analysis, the simulation of the inspection of this defect with CW 60° has been performed with ATHENA : a good agreement with experiment has then been obtained.

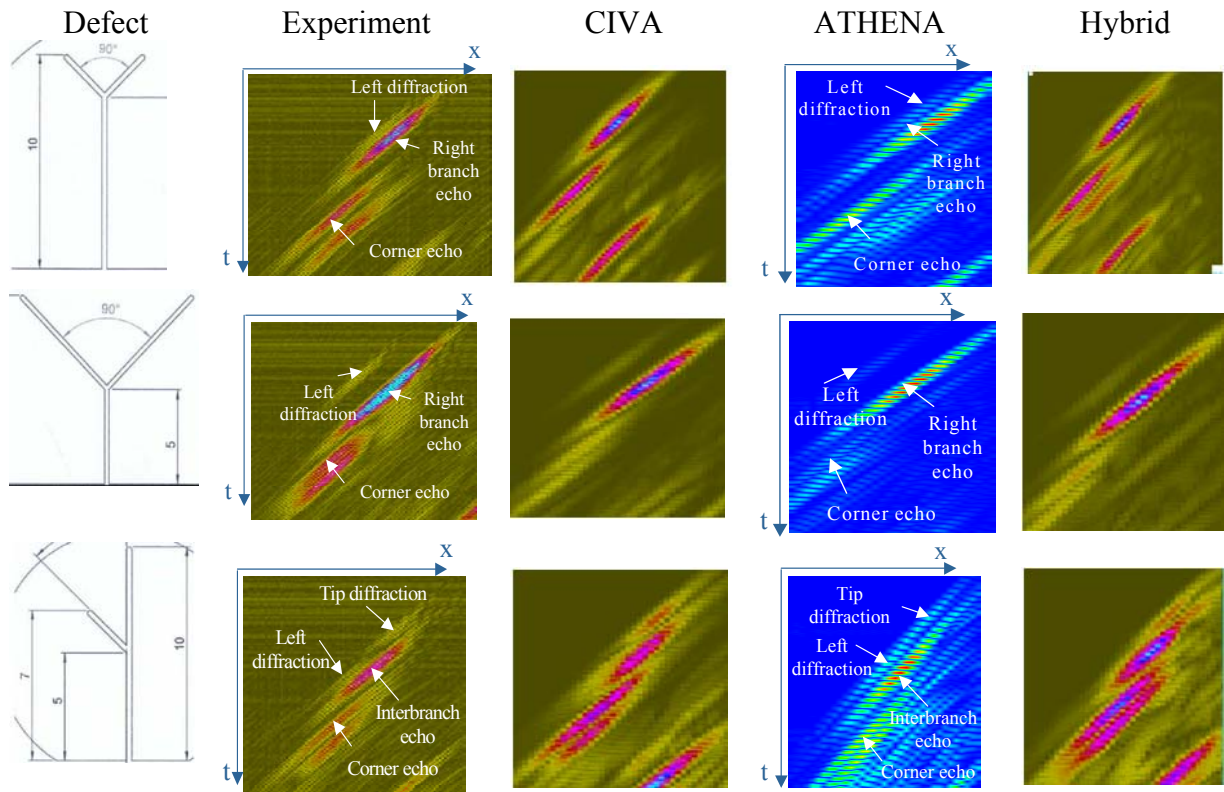


Figure 7 : Comparison of experimental and modelling B-scan images for 45° CW contact transducer (defects E, F and G).

In the case of Y shape defects, the amplitude of the specular echo with the right branch is well estimated. The tip diffraction on the left branch is always detected but is in general underestimated, up to 5.5 dB with the hybrid code on defect F.

For the defect G, composed of a secondary branch connected to a notch, we observed a difficulty to separate the tip echo diffracted by the secondary branch from the inter branch echo (with CIVA and the hybrid code) because of a difference in the temporal resolution of the experimental and simulated transducers. Finally, this last echo is underestimated with CIVA. Some works are in progress to understand and to solve this discrepancy for an echo resulting of multiple reflections between branches.

Table III : Estimated amplitude for branched defects (dB) with CW 45°.

Echo	Test	CIVA	ATHENA	Hybrid	Defect
<i>Defect E</i>					
Corner	3.0	4.5	2.5	4.0	
Left branch	-8.0	-9.0	-11.0	-9.0	
Right branch	7.0	5.5	4.0	5.0	
<i>Defect F</i>					
Corner	3.0	1.5	-2.5	2.0	
Left branch	-8.0	-10.5	-10.5	-10.5	
Right branch	14.0	14.0	12.5	13.5	
<i>Defect G</i>					
Corner	0.5	1.0	-1.5	1.5	
Left branch	-11.0	ND*	-10.0	ND*	
Right branch	-9.0	-9.0	-10.5	-9.5	
Inter branch	3.4	-2.0	1.2	1.0	

* ND : echo not detected

5. CONCLUSIONS

This paper presents the recent developments concerning the simulation of complex flaw scattering. It is focused on multi faceted and branched defects, supposed to represent the morphological specificity of a stress corrosion crack. The investigation, limited to 2D configurations, has been performed for three codes: CIVA UT simulation semi-analytical code, ATHENA 2D finite element code and a recent 2D hybrid code coupling semi-analytical and finite element codes. It has been demonstrated that for CW the codes reproduce quite well the experimental results. Qualitatively, the echoes generated by the complex flaws (corner echoes, diffraction echoes, inner branch reflexions) are observed with the different codes and, for most cases, quantitatively predicted. But some differences in amplitude between experimental data and the different simulation codes are sometimes observed. Such amplitude discrepancies between simulations and experiments may be due to inaccurate description of the probe, small differences between 2D and 3D configurations, or limitations of the models. Works in progress include the analysis of those cases, as well as experiments and simulation for shear waves inspections of those complex flaws with 45° and 60° oblique waves. 3D modelling is also in progress.

6. REFERENCES

- 1) Economou J, Assice A. Cattant F., Salin J. and Stindel M., “Contrôles et expertises métallurgiques de traversés de couvercle de cuve », Fontevraud III Conference, edited by SFEN (French Nuclear Energy Society), 1994.
- 2) Bibollet C., Beroni C., Rimbault S., Stindel M., Verdière N. and Gauchet J-P., “EDF field experience on steam generator divider plate examinations”, Fontevraud 6 Conference, edited by SFEN (French Nuclear Energy Society), 2006.
- 3) Dupond O., Duwig V. and Fouquet T., “Influence of stress corrosion crack morphology on ultrasonic examination performances”, *Review of Progress in QNDE*, 2008 28A 89-96.
- 4) Gengembre N., Lhémy A., Omote R., Fouquet T. and Schumm A., “A semi-analytic-FEM hybrid model for simulating UT configurations involving complicated interactions of waves with defects”, *Review of Progress in QNDE*, 2004 23 74-80.
- 5) Gengembre N., “Pencil method for ultrasonic beam computation”, *5th World Congress on Ultrasonics, Paris*, 2003 1533-1536.
- 6) Raillon R. and Lecœur-Taïbi I., “Transient Elastodynamic Model for Beam Defect Interaction. Application to NonDestructive Testing”, *Ultrasonics*, 2000 38 527-530.
- 7) Becache E., Joly P. and Tsogka C., “A new family of mixed finite elements for the linear elastodynamic problem”, *SIAM J. Numer Anal*, 2002 39(6) 2109-32.
- 8) Chassignole B., Dupond O., Doudet L., Duwig V. and Etchegaray N., “Ultrasonic examination of an austenitic weld : illustration of the disturbance of the ultrasonic beam”, *Review of Progress in QNDE*, 2008 28B 1886-1893.
- 9) Chassignole B. Duwig V., Ploix M.A., Guy P. El Guerjouma R., “Modelling the attenuation in the ATHENA finite element code for ultrasonic testing of austenitic stainless steel welds”, *Ultrasonics*, to be published.
- 10) Mahaut S., Leymarie N., Bonnet-Ben Dhia A.S., Joly P., Rodriguez J., Fouquet T., Rose C., Foucher F., “Projet MOHYCAN : Modélisation hybride et couplage semi-analytique pour le CND ultrasonore”, COFREND Toulouse 2008.
- 11) Auld B.A., “General electromechanical reciprocity relations applied to the calculation of elastic wave scattering coefficients”, *Ultrasonics*, 1979 1 4-10.